Polymer Chemistry

Furry nanoparticles: Synthesis and characterization of nanoemulsion-mediated core crosslinked nanoparticles and their robust stability in vivo

Journal:	*Polymer Chemistry*
Manuscript ID	PY-ART-04-2020-000610.R2
Article Type:	Paper
Date Submitted by the Author:	23-Jun-2020
Complete List of Authors:	Tanaka, Rena ; University of Kitakyushu Fujii, Shota; University of Kitakyushu, Matsuno, Jun; University of Kitakyushu Arai, Koichi; University of Kitakyushu Soejima, Miyo; University of Kitakyushu Lee, Ji Ha; Hiroshima University, Department of Chemical Engineering, Graduate School of Advanced Science and Engineering Takahashi, Rintaro; University of Kitakyushu, Department of Chemistry and Biochemistry Sakurai, Kazuo ; University of Kitakyushu, Dep. of Chemistry & Biochemistry

ARTICLE

Furry nanoparticles: Synthesis and characterization of nanoemulsion-mediated core crosslinked nanoparticles and their robust stability *in vivo*

Received 00th January 20xx,
Accepted 00th January 20xx

DOI: 10.1039/x0xx00000x

Rena Tanaka, Koichi Arai, Jun Matsuno, Miyo Soejima, Ji Ha Lee, Rintaro Takahashi, Kazuo Sakurai*, and Shota Fujii*

Reinforcement of the *in vivo* structural stability of polymer-based nanoparticles such as polymeric micelles has been achieved via covalently crosslinked structures. Herein, we report new core crosslinked nanoparticles prepared via o/w nanoemulsion composed of difunctional polymerizable oil monomers stabilized by a poly(ethylene glycol) (PEG)-bearing surfactant. The obtained PEG-tethered core crosslinked nanoparticles are named furry nanoparticles (f-NPs). The f-NPs' structure was evaluated using light scattering (LS; both static SLS and dynamic DLS), small-angle X-ray scattering, and transmission electron microscopy. The f-NPs' size could be easily controlled by changing the amount of oil monomer, which also affected dye loading and releasing behavior. Employing a disulfide-based oil monomer, we could endow the f-NPs with sensitivity to reduction, demonstrating destabilization in a reducing environment with a high glutathione level matching that in tumors. The structural stability of f-NPs *in vivo* was very high compared with that of a micellar system, resulting in prolonged circulation in the bloodstream. Interestingly, the *in vivo* stability might depend on the crowding density of PEG chains at the outermost surface, even though the structural stability was guaranteed by the crosslinked structure. This study demonstrates the promising synthesis of core crosslinked nanoparticles and their potential as drug carriers.

Introduction

Many types of polymer-based nanoparticle have been designed and developed as drug carriers, especially for tumor tissues, since their size is in an adequate range (10–100 nm) for using a passive targeting strategy based on an enhanced permeability and retention (EPR) effect.[1, 2] Among the polymer-based nanoparticles, polymeric micelles composed of amphiphilic block copolymers have been well studied as potential drug carriers.[2-9] When designing polymeric micelles, tethering poly(ethylene glycol) (PEG) onto the micelle is frequently employed due to its high biocompatibility, endowing the micelle with stealth effects for evading clearance by the reticuloendothelial system (RES) *in vivo*.[10-13] In fact, PEG-tethered polymeric prodrug micelles show relatively prolonged blood circulation, resulting in the enhancement of EPR effects with the suppression of side effects. However, the polymeric micelles do not show the expected superior therapeutic performance relative to naked drugs,[14, 15] which is primarily due to the dynamic properties of the micellar structure. Supramolecular self-assembly systems such as micelles are in thermodynamic equilibrium between the amphiphilic unimer and the micelle.[16] After intravenous (i.v.) administration of the micelles into the bloodstream, most of the encapsulated drugs are released via dissociation of the micelle into unimers owing to the extreme dilution effects, high shear stress in blood vessels, and interactions with plasma proteins and other biomacromolecules.[17-20] This premature drug release is called the initial burst drug release, which is unavoidable even with PEG-tethered micelles.[20-22]

To address this issue, crosslinked polymeric micelles in which the core or shell moiety is covalently crosslinked have been developed and demonstrated reinforced structural stability *in vivo*.[23-26] Pioneering work for the preparation of core crosslinked polymeric micelles in aqueous solution systems was performed by Kataoka et al.[27] They synthesized an amphiphilic block copolymer containing a methacrylate group at the end of the hydrophobic block. After micellization using the copolymer, radical polymerization was conducted and produced a core crosslinked micelle. There are many reported examples of the design of a crosslinking structure prepared via combining hydrophobic blocks using radical polymerization[28-30] or difunctional crosslinking reagents.[31, 32] The endowment of crosslinked micelles with some smart functions such as controlled release under specific conditions was demonstrated by crosslinking via a biosignal-responsive crosslinker, for example, pH cleavable linker,[33] disulfide bonds,[34, 35] and hydrolysable ester bonds.[36] However, as a potential problem in the crosslinking strategy, a transition in the morphology including shape and size would occur during the formation of crosslinking network structures. Furthermore, when demanding control of particle size, each hydrophilic and hydrophobic block must be tuned and optimized for the desired hydrophilic and hydrophobic balance according to the packing parameter theory in micellar systems.[37]

In this paper, we provide a new precise method for the synthesis of nanoemulsion-mediated core crosslinked nanoparticles. We first prepare o/w nanoemulsions, in which the oil phase is composed of bifunctional polymerizable monomers such as divinyl benzene (DVB), stabilized with a PEG-bearing surfactant containing a

Department of Chemistry and Biochemistry, University of Kitakyushu, 1-1 Hibikino, Kitakyushu, Fukuoka 808-0135, Japan.

Electronic Supplementary Information (ESI) available: Synthesis procedure of $PEG_{2k}C_{12}MA$, ^{1}H-NMR spectra, summary of dn/dc, CMC determination, DLS results, SAXS analysis. See DOI: 10.1039/x0xx00000x

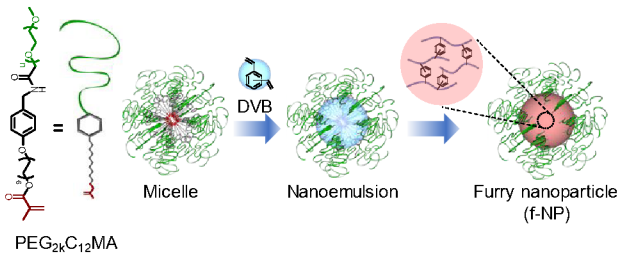

Scheme 1. Schematic illustration of the procedure of synthesizing furry nanoparticles through the formation of nanoemulsion.

methacrylate group at the end of the alkyl chain. Once the radical polymerization is initiated in the nanoemulsion core, crosslinked structures are immediately formed involving the surfactant located at the emulsion surface, resulting in the formation of PEG-tethered core crosslinked nanoparticles capturing the nanoemulsion structure (Scheme 1). Unlike the reported method for the formation of crosslinked structure via employing chemical reactions between hydrophobic blocks or involving a small molecule crosslinker [38,39], the encapsulated DVB itself forms the crosslinked structure while anchoring the surfactant on the surface. Moreover, because radical polymerization is employed to form the crosslink structure, the reaction can be completed instantly, producing the desired core crosslinked nanoparticles easily. The structure of the produced nanoparticles was carefully evaluated using dynamic and static light scattering (DLS and SLS) and small-angle X-ray scattering (SAXS) techniques. We also evaluated the loading and releasing behavior of a dye *in vitro* and pharmacokinetics *in vivo* for the nanoparticles to demonstrate their potential as drug carriers.

Experimental

Material and Synthesis. All chemical reagents were purchased from Tokyo Chemical Industry Co. and Sigma-Aldrich Co., which were used without further purification. All chemical reactions were performed under a nitrogen atmosphere. The progress of the reactions was monitored using thin-layer chromatography (TLC) and detected using ultraviolet (UV; 254 nm) irradiation. Nuclear magnetic resonance (NMR) spectra were recorded with a 500 MHz JEOL spectrometer using chloroform-d as a solvent. The detailed procedure of synthesizing the PEG-bearing surfactant is provided in the Supporting Information.

Preparation of the solution of micelles and core crosslinked nanoparticles. The chloroform solution dissolving the PEG-bearing surfactant was dried in a vacuum to form a film, and then we added 150 mM aqueous NaCl, giving a micellar solution. The concentration of the micellar solution was always set to be 5.0 mg/mL. When loading other molecules into the micelles, we dissolved the compounds with the surfactant in chloroform in advance. For preparing the solution of core crosslinked nanoparticles, we first added a few microliters of acetonitrile solution dissolving DVB into the micellar solution, and then a few milligrams of potassium persulfate (KPS). The mixture solution was vigorously stirred with a probe-type ultrasonic homogenizer (Model UH-50; SMT Co. Ltd., Tokyo, Japan) for 1 min at 60°C. The solution was next mildly stirred for another 30 min at 60°C to complete the radical polymerization, and then purified by spin dialysis.

DLS Measurements. DLS measurements were performed for the micelle and core crosslinked nanoparticle solutions in 150 mM aqueous NaCl on a Beckman-Coulter DelsaMax instrument at 25°C at a scattering angle of 171°.

Transmission Electron Microscopy (TEM) Observation. We placed a droplet of the solution of core crosslinked nanoparticles (5.0 mg/mL in 150 mM aqueous NaCl) on a TEM grid coated with elastin carbon film. After 1 min, the droplet was swabbed with filter paper. Another droplet of Nano-W (Nanoprobes, aq. 2% w/v) was then mounted on the grid and swabbed immediately. The grid was dried and then loaded into a JEOL JEM-2100Plus electron microscope with an accelerating voltage of 200 kV.

SAXS Measurements. SAXS measurements were performed at the BL-40B2 beamline of the SPring-8 facility, Hyōgo Prefecture, Japan. A digital detector (Pilatus-100K) was placed at 1 or 4 m from the sample. The wavelength of the incident beam (λ) was adjusted to 0.10 nm. This set-up provided a q range of 0.050–6.0 nm^{-1}, where q is the magnitude of the scattering vector, defined as $q = 4\pi \sin\vartheta/\lambda$, with a scattering angle of 2ϑ. The X-ray transmittance of the samples was determined by using ion chambers located in front of and behind each sample. The detailed experimental procedures are reported elsewhere. The absolute SAXS intensities were recorded using the absolute scattering intensity of water.[40]

We used a hard sphere model for fitting the SAXS profiles of the micelles and the f-NPs. The model can be described by the following expression:

$$I(q)_{\mathrm{HS}} = \left\{3V\Delta\rho\frac{j_1(qR)}{qR}\right\}^2 \#(1)$$

R and V are the radius and volume of the particle, respectively. $\Delta\rho$ and j_1 are the electron density contrast and the second spherical Bessel function, respectively. For core crosslinked nanoparticles, we modified the hard sphere model by adding the Ornstein-Zernike (OZ) equation, which can be considered to represent independent scattering when the correlation length ξ is small enough compared with the particle size.[41] The modified model is described as follows:

$$I(q)_{\mathrm{HS-OZ}} = \left\{3V\Delta\rho\frac{j_1(qR)}{qR}\right\}^2 + \frac{I_{OZ}(0)}{1+q^2\xi^2}\#(2)$$

Here, $I_{OZ}(0)$ is a constant. The SAXS profiles in the low-q region follow the Guinier equation:

$$I(q) = I(0)\exp\left(-\frac{q^2R_g{}^2}{3}\right)\#(3)$$

where $I(0)$ is the forward scattering intensity at $q = 0$ and the radius of gyration (R_g) is determined from the slope of the $\ln[I(q)]$ vs. q^2 plot (Guinier plot).

Asymmetrical flow field flow fractionation coupled with multi-angle light scattering (MALS) and quasi-elastic light scattering (QELS) measurements. Sample solution (60 μL) was injected into an Eclipse 3+ separation system (Wyatt Technology Europe GmbH, Dernbach, Germany) for the system of AF4 at 25°C. A 5 kDa regenerated cellulose membrane was attached at the bottom of a Wyatt channel (Eclipse 3 channel LC) for the measurements. The fractionated solution was then passed sequentially through a UV detector, a Dawn Heleos II MALS detector (Wyatt Technology), a QELS autocorrelator (Wyatt Technology), and an Optilab rEX DSP differential refractive index (RI) detector (Wyatt Technology), operating at a wavelength of 658 nm. The cross-flow was exponentially decreased from 3.0 to 0 mL/min over the measurement time. The specific refractive index increments ($\partial n/\partial c$) of the samples dialyzed against 150 mM aqueous NaCl were determined using a DRM-1021 differential refractometer (Otsuka Electronics, Osaka, Japan) (see Table S1).

Study of reduction sensitivity for f-NPs with a disulfide crosslinker. In this experiment, f-NPs were prepared using mixed two crosslinkers: DVB and bis(2-methacryloyl)oxyethyl disulfide at the

molar ratio of 1:1. The obtained f-NPs composed of the disulfide crosslinker are denoted by f-NPs^{DC}. The f-NP^{DC} was incubated in 150 mM aqueous NaCl with or without 10 mM GSH for 1 h. For the sample solution containing GSH, the solution was replaced with pure 150 mM aqueous solution by spin dialysis, then THF was added into the solution before measuring DLS.

Release study of pyrene from f-NPs with a disulfide crosslinker. Sample solutions of the f-NP^{DC} containing pyrene were dialyzed in 150 mM aqueous NaCl at 37°C. The inside solution was taken, and then pyrene aggregates was removed by centrifugation at 13,000 g for 10 min at 4°C. The supernatant was analyzed by UV-vis measurements using a UV-vis spectrophotometer (JASCO V-630; Jasco, Tokyo, Japan).

***In vivo* Pharmacokinetic Experiments**. All animal procedures were performed in accordance with the Guidelines for Care and Use of Laboratory Animals of the University of Kitakyushu and approved by the Animal Ethics Committee of the University of Kitakyushu. All samples included a nitrobenzoxadiazole (NBD)-labeled lipid (NBD-L) as a fluorescent probe. The sample solution was injected into BALB/c mice (n = 5, male, 7–8 weeks, BW = 23 g; Sankyo Labo Service Corporation, Tokyo, Japan) via the tail vein. At various times, blood samples were taken from the eye socket vein. The plasma was separated by centrifugation at 1200 g for 15 min at 4°C, and then the fluorescence of the sample was measured.

Statistical Analysis. The statistical analysis was performed using *t*-test and analysis of variance. All data are shown as mean ± standard deviation (S.D.).

Results and Discussion

Preparation of Nanoemulsion-mediated Core Crosslinked Nanoparticles using a Polymerizable Surfactant Bearing PEG

A polymerizable surfactant bearing PEG as a hydrophilic group and a methacrylate group attached at the end of the hydrophobic alkyl chain (denoted as $PEG_{2k}C_{12}MA$) was synthesized via Scheme S1. The chemical structures of precursors (compounds I and II) were confirmed by ^{1}H-NMR and mass spectroscopy. PEG (2000 g/mol) bearing N-hydroxylsuccinimide was reacted with compound II bearing an amine to produce compound III, which was then purified by reprecipitation. The hydroxyl group at the end of the alkyl chain of compound III was reacted with methacryloyl chloride, giving the final compound, $PEG_{2k}C_{12}MA$. The chemical structure of the PEGylated compounds was confirmed by ^{1}H-NMR (see Supplementary Information). The critical micelle concentration (CMC) of $PEG_{2k}C_{12}MA$ micelles was determined using 8-Anilinonaphthalene-1-sulfonate (ANS) as a fluorescent probe to be 5.0 μM (0.11 mg/mL) in 150 mM aqueous NaCl (Fig. S1). All following experiments were carried out at the above CMC.

The nanoemulsion-mediated core crosslinked nanoparticles were prepared via Scheme 1. The solution of $PEG_{2k}C_{12}MA$ micelles was mixed with DVB and KPS, and then the solution was vigorously stirred using a probe-type ultrasonic homogenizer for 1 min at 60°C, which induced a radical polymerization reaction while forming nanoemulsion stabilized by the surfactant. Owing to the bifunctional polymerizable group in DVB, the reaction provided crosslinked structures involving the hydrophobic moiety of $PEG_{2k}C_{12}MA$. Since the prepared nanoparticles were no longer micelles, and the PEG chains were tethered on the crosslinked nanoparticles, we named them furry nanoparticles: f-NPs$_{\varphi\#}$, where φ# represents the molar ratio of DVB to $PEG_{2k}C_{12}MA$: [DVB]/[$PEG_{2k}C_{12}MA$].

Fig. 1a shows ^{1}H-NMR spectra of $PEG_{2k}C_{12}MA$ micelles and f-NPs$_{\varphi10}$ in 150 mM aqueous NaCl in D_2O. The vinyl peak of the methacrylate group disappeared after conducting the polymerization reaction, indicating that the whole of the

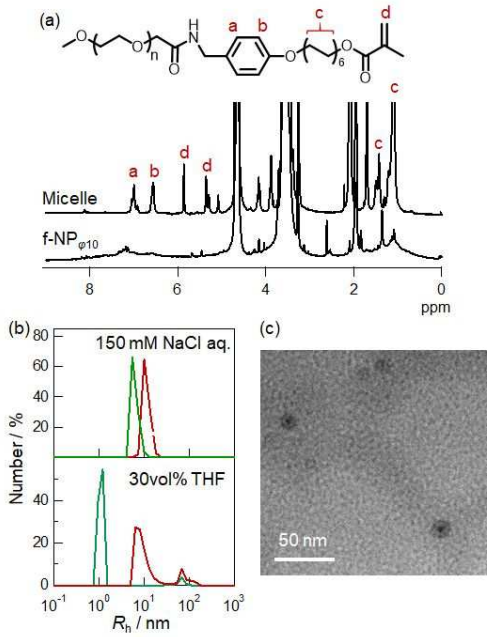

Fig. 1 (a) ^{1}H-NMR spectra of $PEG_{2k}C_{12}MA$ micelles and f-NPs$_{\varphi10}$ in 150 mM aqueous NaCl in D_2O. (b) DLS histograms of $PEG_{2k}C_{12}MA$ micelles (green lines) and f-NPs$_{\varphi10}$ (red lines) in 150 mM aqueous NaCl (upper) or 30vol% THF (lower). (c) TEM image of f-NPs$_{\varphi10}$.

hydrophobic moiety of $PEG_{2k}C_{12}MA$ was involved in the crosslinked structure. The peaks around 1.0 and 7.0 ppm assigned as benzene and alkyl chains of $PEG_{2k}C_{12}MA$, respectively, broadened markedly after the polymerization. This indicates that the mobility of the hydrophobic moiety was restricted in the crosslinked structure, suggesting that the crosslinked core involved the benzene moiety as well as the alkyl chain.

Fig. 1b presents a DLS histogram comparing $PEG_{2k}C_{12}MA$ micelles and f-NPs$_{\varphi10}$ in 150 mM aqueous NaCl. The hydrodynamic radii (R_h) of the micelles and f-NPs$_{\varphi10}$ were 6.3 and 13 nm, respectively. The increment in the particle size was presumably due to that the surfactant aggregation number increased by encapsulating DVB into the micellar core, meaning the formation of nanoemulsions, whose structure were then captured by radical polymerization. The TEM image of f-NPs$_{\varphi10}$, shown in Fig. 1c, displays a spherical morphology with a core-shell structure, indicating the dense structure of the crosslinked core compared with that of the shell part. After adding THF, which is a good solvent for $PEG_{2k}C_{12}MA$, into the micellar solution, the micellar structure collapsed, while f-NPs$_{\varphi10}$ did not change much in size. This strongly suggested the high structural stability of f-NPs compared with that of the micelles. The R_h of f-NPs can be controlled by changing the φ because f-NPs are formed through the nanoemulsion whose size depends on φ (Fig. S2). Although the R_h could be controlled when φ < 12, large aggregates were formed (R_h > 100 nm) and the solution became opaque at φ > 12. This was presumably due to the coverage ratio of the hydrophobic core with PEG chains decreasing at high φ, resulting in the formation of an aggregate by hydrophobic interactions between the particles.

Structural Characterization of f-NPs Based on Light Scattering and SAXS Measurements

Fig. 2a shows a fractogram of AF4-MALS-UV for $PEG_{2k}C_{12}MA$ micelles and f-NPs in 150 mM aqueous NaCl. The micelle peak

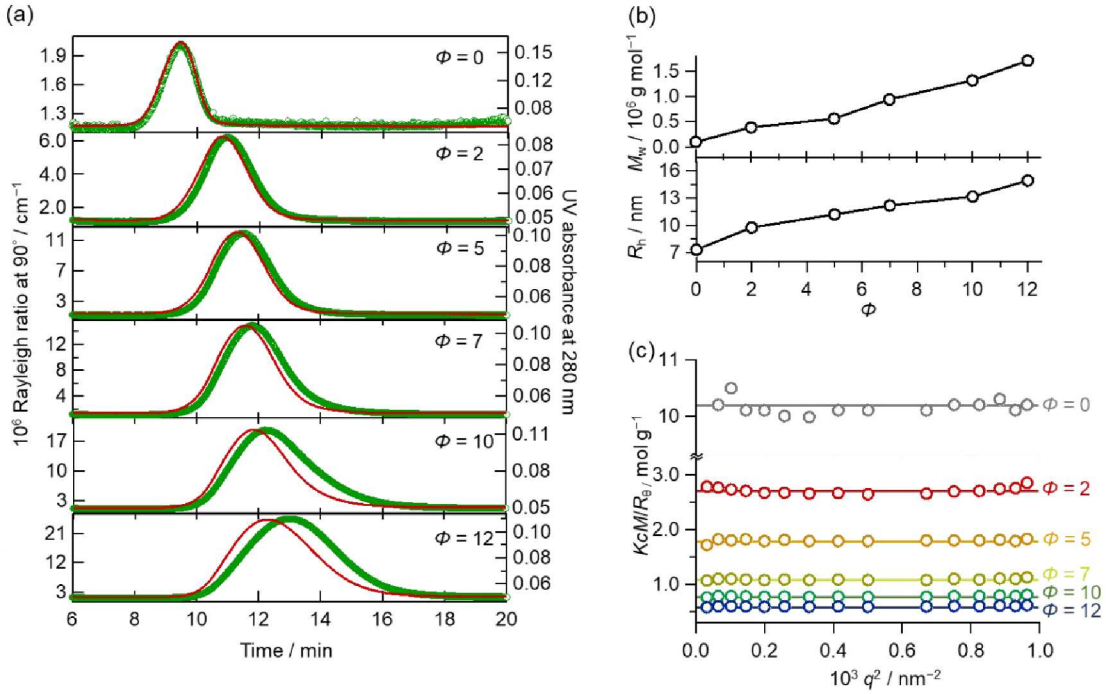

Fig. 2 (a) AF4-MALS fractograms of $PEG_{2k}C_{12}MA$ micelles and f-NPs in 150 mM aqueous NaCl. The green points and red lines are the light scattering intensity at 90° and UV absorbance at 280 nm, respectively. (b) M_w and R_h plotted against φ {= [DVB]/[$PEG_{2k}C_{12}MA$]}. (c) Zimm plots for $PEG_{2k}C_{12}MA$ micelles and f-NPs at the peak top of the fractogram.

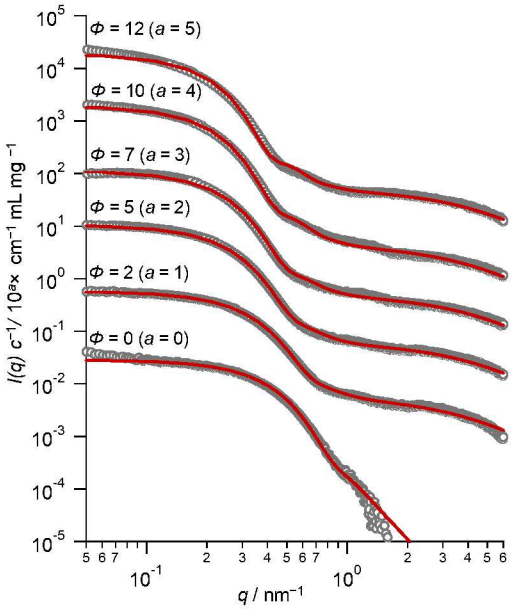

Fig. 3 SAXS profiles (gray points) of $PEG_{2k}C_{12}MA$ micelles and f-NPs in 150 mM aqueous NaCl and theoretical curves (red lines) calculated using the core-shell sphere model (eq. 1) or the modified core-shell sphere model with Ornstein-Zernike function (eq. 2).

appeared faster than that of f-NPs. In the system of AF4, larger particles are eluted later than smaller ones.[42] This means that f-NPs were larger than micelles, and the size of f-NPs gradually increased with increasing φ. This is also supported by the R_h values determined at the peak top of each fractogram (Fig. 2b). The weight-averaged molar masses (M_w) of the micelles and f-NPs were determined from the Zimm plot shown in Fig. 2c. The values of R_h and M_w are summarized in Table 1. M_w also increased with increasing φ, which is the same behavior as that of particle size.

Table 1. Summary of R_h and M_w determined with AF4-MALS-QELS and R, ξ, and R_g determined by the analysis of SAXS profiles.

	AF4-MALS-DLS		SAXS		
φ	R_h [nm]	M_w [10^5 g/mol]	R [nm]	ξ [nm]	R_g [nm]
0	7.31	1.01	4.25	-	4.28
2	9.75	3.87	5.15	0.26	5.09
5	11.2	5.60	6.70	0.26	6.88
7	12.2	9.39	7.60	0.26	7.00
10	13.2	13.2	8.90	0.26	8.55
12	14.9	17.1	9.50	0.26	10.0

Fig. 3a shows the SAXS profiles of $PEG_{2k}C_{12}MA$ micelles and f-NPs in 150 mM aqueous NaCl. The slope at the low-q region satisfies the relationship of $I(q) \propto q^0$ in all SAXS profiles, indicating the presence of isolated spherical particles without any secondary aggregates.[43, 44] For the SAXS profile of the micelles, the scattering intensity at the high-q region followed the power law of q^{-4}. This indicates that the micelle–water interface is sharp and smooth according to the Porod law.[43, 44] The SAXS profile can be reproduced using a hard sphere model (eq. 1), the fitting parameters of which are summarized in Table 1. Micelle structures can normally be described by a core-shell model consisting of two phases, hydrophobic core and hydrophilic shell, in SAXS analysis.[45] However, since oscillation at the high-q region was not clearly observed in the SAXS profile, the core radius and shell thickness could not be

determined accurately, resulting in being overestimated. Therefore, the simple hard sphere model was adopted. The radius of the micelle was 4.25 nm, which is smaller than that determined by DLS. This is because of the low contrast between the PEG and water, limiting the ability to estimate the shell thickness accurately.[46]

In contrast to the micellar system, the SAXS profiles of f-NPs did not follow the Porod law. This is presumably due to the crosslinked structure in the particle core, whose scattering can be described by the Ornstein-Zernike function.[47] Those SAXS profiles could be reproduced using a modified hard sphere model (eq. 2), the fitting parameters of which are listed in Table 1. The ξ corresponding to the mesh size in the core was very small (~0.26 nm) and did not differ greatly among all f-NPs. This is because the crosslinked core is tightly packed due to hydrophobic interactions. The q value at the first minimum in the SAXS oscillation of f-NPs was slightly smaller than that of the micelles and became smaller with increasing φ, indicating that the size of the f-NPs was increasing with φ. The radius (R) determined by fitting and the radius of gyration (R_g) estimated by Guinier plot (Fig. S3) of the f-NPs actually increased with φ, which is consistent with the DLS results.

Controlling the Loading Ratio and Release Behavior of a Dye *In vitro* and Sensitivity to Reduction of f-NPs Composed of Disulfide-based Crosslinker

The f-NPs can encapsulate hydrophobic molecules in their core, just like micellar systems. Fig. 4a shows the UV spectra of the $PEG_{2k}C_{12}MA$ micelle (φ = 0) and f-NPs at different φ after loading pyrene. As shown in the figure, the absorbance at 340 nm according to pyrene absorption increased with increasing φ. Fig. 4b shows the dependence of φ on the loading ratio (LR) of pyrene into the f-NPs. For the micelles (φ = 0), the LR was very small at about 0.2%, while f-NPs improved the LR that can be controlled by φ, reaching about 3.6% at φ = 12. This relatively high LR of f-NPs might surpass this characteristic of nanoemulsions whose drug LR can also be controlled by changing the emulsion size.[48]

Encapsulated molecules into crosslinked structures such as f-NP' core are physically trapped in the structure, results in not being released at desired location *in vivo*, which will be problem in practical drug delivery. In other systems of core crosslinked nanoparticles, this issue has been resolved by conferring sensitivity to reduction on crosslinked structures.[23] In the intracellular matrix of tumor tissues, glutathione (GSH), which is a tripeptide that can reversibly cleave disulfide bonds, is overexpressed at around 10 mM, which is a concentration about 10 times higher than that in normal tissues.[49] When internalizing the reduction-sensitive core crosslinked nanoparticles containing disulfide bonds into the cytosol of cancer cells, the crosslinked structure would be cleaved by GSH and subsequently release the encapsulated drugs. Being composed of disulfide bonds in the crosslinked structure, the structure of f-NPs would also be destabilized by GSH, as shown in the schematic in Fig. 5.

We modified the crosslinked structure by mixing DVB with disulfide-based dimethacrylate, bis(2-methacryloyl)oxyethyl disulfide to produce f-NPs composed of the disulfide crosslinker (f-NPs^{DC}). After incubating the f-NP^{DC} solution in 150 mM aqueous NaCl containing 10 mM GSH for 1 h, the sensitivity to reduction was investigated using DLS measurements. The particle sizes of f-NPs^{DC} in aqueous system with or without GSH were around 9.5 and 11 nm, respectively (Fig. 5a), whereas large aggregates (~100 nm) were immediately formed when adding THF into the f-NP^{DC} solutions incubated with GSH (Fig. 5b). This was presumably due to GSH cleaving the disulfide bonds in the crosslinked structure, allowing the hydrophobic part to be exposed to the solvent phase in THF/water solutions and leading to the formation of the large aggregate. Figure 5c shows the profile of release of pyrene from $PEG_{2k}C_{12}MA$ micelles

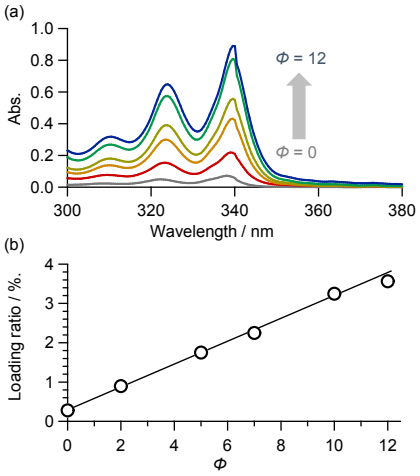

Fig. 4 (a) UV spectra of f-NPs containing pyrene at different φ {= [DVB]/[$PEG_{2k}C_{12}MA$]} (φ = 0: gray, φ = 2: red, φ = 5: orange, φ = 7: yellow, φ = 10: green, φ = 12: blue). (b) Loading ratio of pyrene into f-NPs plotted against φ.

and the f-NPs^{DC} with or without GSH. Although micelles released pyrene about 50% after 12 hours, the release was suppressed to about 35% in the system of the f-NP^{DC}. The physical trapping by the crosslinked structure in the particle core contributed the higher retention ability for the encapsulated molecule. However, when incubating the f-NP^{DC} with GSH, the release was enhanced to about 55% which was close to that of the micellar system. This is presumably due to the cleavage of the disulfide bonds in the crosslinked core by GHS. These results suggest the potential of f-NPs for practical use as drug carriers by modifying the core.

The Effect of the Structural Characteristics of f-NPs on Their Pharmacokinetics *In vivo*

To monitor the pharmacokinetics of $PEG_{2k}C_{12}MA$ micelles and f-NPs, we used a nitrobenzoxadiazole (NDB)-labeled lipid (NDB-L) as a probe. We assumed that the elimination of the NDB-L fluorescence after i.v. administration represents the dissociation and clearance of those nanoparticles *in vivo*. Fig. 6 shows the pharmacokinetic profile of the micelles and f-NPs. The micelles were quickly cleared after administration. This must have been due to the initial burst caused by the unstable dynamic structure of the micelles, as mentioned in the introduction. On the other hand, f-NPs demonstrated prolonged blood circulation *in vivo* due to the enhanced particle stability resulting from the crosslinked structure. When comparing f-$NPs_{\varphi5}$ and f-$NPs_{\varphi10}$, the survival rate of f-$NPs_{\varphi10}$ at 24 h post-injection was about 50%, which was better than that of f-$NPs_{\varphi5}$ (~25%). This difference is presumably attributable to two factors. One relates to the retention ability of NBD-L in their crosslinked structures, which depends on the crosslink density. NBD-L was physically trapped in the structure and their crosslink density somehow might rely on φ. Many factors can destabilize the particle structure *in vivo*, such as various plasma proteins and high shear stress in blood vessels, which might pull NBD-L molecules out from the f-NPs. The other potential factor relates to the PEG density in the particle shell. To suppress the interaction with plasma proteins *in vivo*, the PEG chain conformation must be controlled.[50, 51] We can estimate the PEG density at the

outermost surface (D_{OS}) of nanoparticles using the following equation.[52]

$$D_{OS} = N_{c,PEG}\pi(R_{g,PEG})^2/4\pi R^2 \#(4)$$

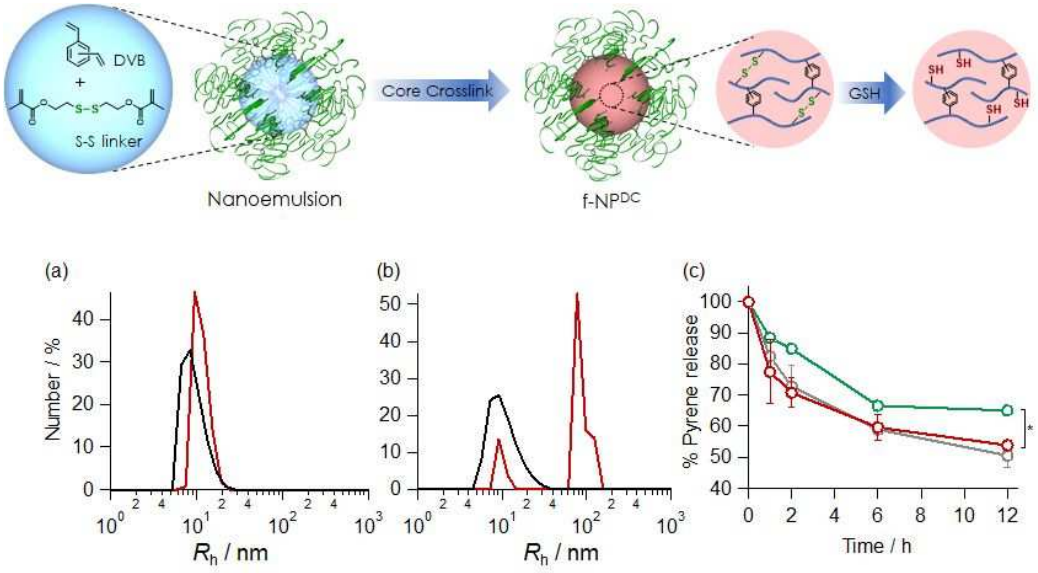

Fig. 5 DLS histograms of f-NP^{DC} in 150 mM aqueous NaCl (a) or 30vol% THF (b). The black and red solid lines in the histograms indicate before and after incubation with 10 mM GSH for 1 h, respectively. (c) *In vitro* pyrene release profile from $PEG_{2k}C_{12}MA$ micelles (gray) and f-NPs^{DC} in 150 mM NaCl aqueous solution with (red) or without (green) 10 mM GSH at 37°C. The symbol * indicates *p*-value < 0.05.

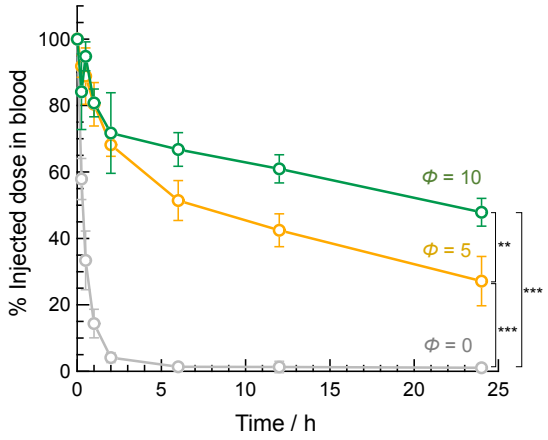

Fig. 6 Time dependence of the concentration of NDB-L involved in $PEG_{2k}C_{12}MA$ micelles (gray), f-NPs$_{\varphi 5}$ (yellow), and f-NPs$_{\varphi 10}$ (green) after i.v. administration into mice. The dye concentration in blood at 1 min after injection was set as 100%. The symbol ** and *** indicates *p*-value < 0.01 and 0.001, respectively.

$N_{c,PEG}$ and R are the number of PEG chains and the particle size, respectively. $R_{g,PEG}$ is the radius of gyration of a free (i.e., in an unperturbed state) PEG single chain with the same molecular weight as a tethered one. In the case of D_{OS} < 1, the tethered PEG chains do not interact with each other at the outermost surface, while the chains were squeezed conformation at the outermost surface when D_{OS} > 1. We have already determined the molar mass of f-NPs and knew the molar ratio of $PEG_{2k}C_{12}MA$ and DVB as φ, giving the values of D_{OS} for f-NPs$_{\varphi 5}$ and f-NPs$_{\varphi 10}$ of 0.91 and 1.27, respectively. The smaller D_{OS} (<1) of f-NPs$_{\varphi 5}$ might allow plasma proteins to penetrate the shell moiety, which would promote the clearance of particles by RES. The higher D_{OS} (>1) of f-NPs$_{\varphi 10}$ indicates the crowding structure of PEG chains in the shell, which might help to evade RES clearance and provide the better blood circulation.

Conclusions

In conclusion, we prepared core crosslinked nanoparticles (f-NPs) via nanoemulsions composed of polymerizable oil molecules stabilized with $PEG_{2k}C_{12}MA$ and carefully characterized their structures, mainly using small-angle scattering techniques including AF4-MALS-QELS and SAXS. The advantage of using the nanoemulsion-mediated process is that, first, it is easy to control the particle size in the range of ~6 to ~16 nm by just changing the molar ratio of oil monomers and surfactant. This also helps to control the loading ratio for hydrophobic molecules since the particle core volume for encapsulating such molecules depends on the particle size. Second, we can easily endow f-NPs with a function by employing stimulus-responsive oil monomers. The f-NPs composed of a disulfide-based monomer demonstrated destabilization in the presence of GSH upon sensitivity to reduction of the crosslinked network in the core. The micelles of $PEG_{2k}C_{12}MA$ were very quickly cleared after i.v. administration to mice, while the f-NPs showed prolonged blood circulation *in vivo* due to their high structural stability resulting from their core crosslinked structure. Interestingly, we found that the PEG density at the outermost surface might be important for this prolonged blood circulation even though the particle structure was stabilized by crosslinked structures. We hope that this new technique of using f-NPs would be helpful for designing and improving novel drug carriers.

Conflicts of interest

There are no conflicts to declare.

Acknowledgements

All SAXS measurements were carried out at SPring-8 BL40B2 (Proposal No. 2018A1454, 2018B1396, and 2019B1207). This work was supported by JST CREST Grant Number JPMJCR1521, Japan. This research was supported by a JSPS KAKENHI: Grant-in-Aid for Scientific Research (Grant Number 19K15394), Grant-in-Aid for Scientific Research A (Grant Number 20H00668),and Grant-in-Aid for Challenging Exploratory Research (Grant Number 20K20449).

References

1. J. Fang, H. Nakamura and H. Maeda, *Adv. Drug Deliv. Rev.*, 2011, **63**, 136-151.
2. H. Cabral, Y. Matsumoto, K. Mizuno, Q. Chen, M. Murakami, M. Kimura, Y. Terada, M. R. Kano, K. Miyazono, M. Uesaka, N. Nishiyama and K. Kataoka, *Nat. Nanotechnol.*, 2011, **6**, 815-823.
3. E. Blanco, H. Shen and M. Ferrari, *Nat. Biotechnol.*, 2015, **33**, 941-951.
4. R. Gref, Y. Minamitake, M. T. Peracchia, V. Trubetskoy, V. Torchilin and R. Langer, *Science*, 1994, **263**, 1600.
5. K. Kataoka, A. Harada and Y. Nagasaki, *Adv. Drug Deliv. Rev.*, 2012, **64**, 37-48.
6. H. Otsuka, Y. Nagasaki and K. Kataoka, *Adv. Drug Deliv. Rev.*, 2003, **55**, 403-419.
7. K. Ulbrich, K. Holá, V. Šubr, A. Bakandritsos, J. Tuček and R. Zbořil, *Chem. Rev.*, 2016, **116**, 5338-5431.
8. B. Tyler, D. Gullotti, A. Mangraviti, T. Utsuki and H. Brem, *Adv. Drug Deliv. Rev.*, 2016, **107**, 163-175.
9. K. S. Lee, H. C. Chung, S. A. Im, Y. H. Park, C. S. Kim, S.-B. Kim, S. Y. Rha, M. Y. Lee and J. Ro, *Breast Cancer Res. Treat*, 2008, **108**, 241-250.
10. R. Gref, M. Lück, P. Quellec, M. Marchand, E. Dellacherie, S. Harnisch, T. Blunk and R. H. Müller, *Colloids Surf. B*, 2000, **18**, 301-313.
11. H. Otsuka, Y. Nagasaki and K. Kataoka, *Curr. Opin. Colloid Interface Sci.*, 2001, **6**, 3-10.
12. W. Norde and D. Gage, *Langmuir*, 2004, **20**, 4162-4167.
13. K. Knop, R. Hoogenboom, D. Fischer and U. S. Schubert, *Angewandte Chemie International Edition*, 2010, **49**, 6288-6308.
14. D. L. Stirland, J. W. Nichols, S. Miura and Y. H. Bae, *J. Control Release*, 2013, **172**, 1045-1064.
15. I. H. Park, J. H. Sohn, S. B. Kim, K. S. Lee, J. S. Chung, S. H. Lee, T. Y. Kim, K. H. Jung, E. K. Cho, Y. S. Kim, H. S. Song, J. H. Seo, H. M. Ryoo, S. A. Lee, S. Y. Yoon, C. S. Kim, Y. T. Kim, S. Y. Kim, M. R. Jin and J. Ro, *Cancer Res. Treat.*, 2017, **49**, 569-577.
16. S. C. Owen, D. P. Y. Chan and M. S. Shoichet, *Nano Today*, 2012, **7**, 53-65.
17. J. Liu, F. Zeng and C. Allen, *Eur. J. Pharm. Biopharm.*, 2007, **65**, 309-319.
18. A. B. Ebrahim Attia, C. Yang, J. P. K. Tan, S. Gao, D. F. Williams, J. L. Hedrick and Y.-Y. Yang, *Biomaterials*, 2013, **34**, 3132-3140.
19. Y. Zhao, I. van Rooy, S. Hak, F. Fay, J. Tang, C. d. L. Davies, M. Skobe, E. A. Fisher, A. Radu, Z. A. Fayad, C. de Mello Donegá, A. Meijerink and W. J. M. Mulder, *ACS Nano*, 2013, **7**, 10362-10370.
20. X. Sun, G. Wang, H. Zhang, S. Hu, X. Liu, J. Tang and Y. Shen, *ACS Nano*, 2018, **12**, 6179-6192.
21. H. Chen, S. Kim, W. He, H. Wang, P. S. Low, K. Park and J.-X. Cheng, *Langmuir*, 2008, **24**, 5213-5217.
22. P. Zou, H. Chen, H. J. Paholak and D. Sun, *Mol. Pharm.*, 2013, **10**, 4185-4194.
23. M. Talelli, M. Barz, C. J. F. Rijcken, F. Kiessling, W. E. Hennink and T. Lammers, *Nano Today*, 2015, **10**, 93-117.
24. Y. Li, K. Xiao, W. Zhu, W. Deng and K. S. Lam, *Adv. Drug Deliv. Rev.*, 2014, **66**, 58-73.
25. E. S. Read and S. P. Armes, *Chem. Commun.*, 2007, DOI: 10.1039/B701217A, 3021-3035.
26. R. K. O'Reilly, C. J. Hawker and K. L. Wooley, *Chem. Soc. Rev.*, 2006, **35**, 1068-1083.
27. M. Iijima, Y. Nagasaki, T. Okada, M. Kato and K. Kataoka, *Macromolecules*, 1999, **32**, 1140-1146.
28. W.-C. Lee, Y.-C. Li and I. M. Chu, *Macromol. Biosci.*, 2006, **6**, 846-854.
29. X. Shuai, T. Merdan, A. K. Schaper, F. Xi and T. Kissel, *Bioconjugate Chem.*, 2004, **15**, 441-448.
30. X. Hu, X. Chen, J. Wei, S. Liu and X. Jing, *Macromol. Biosci.*, 2009, **9**, 456-463.
31. M. A. Gauthier, M. I. Gibson and H.-A. Klok, *Angew. Chem Int. Ed.*, 2009, **48**, 48-58.
32. L. Nuhn, M. Hirsch, B. Krieg, K. Koynov, K. Fischer, M. Schmidt, M. Helm and R. Zentel, *ACS Nano*, 2012, **6**, 2198-2214.
33. Y. Wu, W. Chen, F. Meng, Z. Wang, R. Cheng, C. Deng, H. Liu and Z. Zhong, *J. Control Release*, 2012, **164**, 338-345.
34. Y. Li, K. Xiao, J. Luo, W. Xiao, J. S. Lee, A. M. Gonik, J. Kato, T. A. Dong and K. S. Lam, *Biomaterials*, 2011, **32**, 6633-6645.
35. C. Maiti, S. Parida, S. Kayal, S. Maiti, M. Mandal and D. Dhara, *ACS Appl. Mater. Interfaces*, 2018, **10**, 5318-5330.
36. C. J. Rijcken, C. J. Snel, R. M. Schiffelers, C. F. van Nostrum and W. E. Hennink, *Biomaterials*, 2007, **28**, 5581-5593.
37. J.N. Israelachvili, Intermolecular and surface forces. Vol. 450 (Academic press London, 1992).
38. T. K. Bronich, P. A. Keifer, L. S. Shlyakhtenko and A. V. Kabanov, *J. Ame. Chem. Soc.*, 2005, **127**, 8236-8237.
39. J. O. Kim, G. Sahay, A. V. Kabanov and T. K. Bronich, *Biomacromolecules*, 2010, **11**, 919-926.
40. D. Orthaber, A. Bergmann and O. Glatter, *J. Appl. Crystallogr.*, 2000, **33**, 218-225.
41. T. Hashimoto, H. Tanaka, S. Koizumi, K. Naka and Y. Chujo, *J. Appl. Crystallogr.*, 2007, **40**, s73-s77.
42. F. Caputo, J. Clogston, L. Calzolai, M. Rösslein and A. Prina-Mello, *J. Control Release*, 2019, **299**, 31-43.
43. L.A. Feigin, D.I. Svergun, Structure Analysis by Small-Angle XRay and Neutron Scattering; Plenum Press: New York. 1987.
44. O. Glatter, O. Kratky, Small Angle X-ray Scattering. In Small Angle X-ray Scattering; Academic Press: London. 1982.
45. J. S. Pedersen and C. Svaneborg, *Curr. Opin. Colloid Interface Sci.*, 2002, **7**, 158-166.
46. I. Akiba, N. Terada, S. Hashida, K. Sakurai, T. Sato, K. Shiraishi, M. Yokoyama, H. Masunaga, H. Ogawa, K. Ito and N. Yagi, *Langmuir*, 2010, **26**, 7544-7551.
47. H. D. Bale and P. W. Schmidt, *Phys. Rev. Lett.*, 1984, **53**, 596-599.
48. G. Calderó, R. Montes, M. Llinàs, M. J. García-Celma, M. Porras and C. Solans, *Colloid Surf. B*, 2016, **145**, 922-931.
49. G. Saito, J. A. Swanson and K.-D. Lee, *Adv. Drug Deliv. Rev.*, 2003, **55**, 199-215.
50. T. A. Tockary, K. Osada, Q. Chen, K. Machitani, A. Dirisala, S. Uchida, T. Nomoto, K. Toh, Y. Matsumoto, K. Itaka, K. Nitta, K. Nagayama and K. Kataoka, *Macromolecules*, 2013, **46**, 6585-6592.
51. K. Shiraishi, Y. Sanada, S. Mochizuki, K. Kawano, Y. Maitani, K. Sakurai and M. Yokoyama, *J. Control Release*, 2015, **203**, 77-84.
52. S. Fujii, M. Sakuragi and K. Sakurai, in *Control of Amphiphile Self-Assembling at the Molecular Level: Supra-Molecular Assemblies with Tuned Physicochemical Properties for Delivery Applications*, American Chemical Society, 2017, vol. 1271, ch. 5, pp. 115-129.

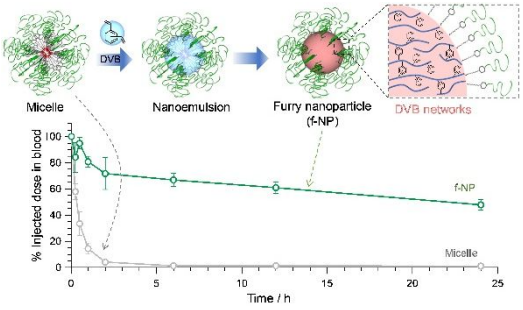

Core crosslinked nanoparticles were prepared via nanoemulsion stabilized by a poly(ethylene glycol)-bearing surfactant, which shows high structural stability in vivo.

Innovation of Advanced Bio- and/or Eco-Materials by Integrating Molecular Biology, Supramolecular Chemistry, Polymer Science, and Synchrotron Small-Angle X-ray Scattering

Sakurai Laboratory

Department of Chemistry and Chemical Engineering

University of Kitakyushu

1-1 Hibikino, Wakamatsu-ku, Kitakyushu, Fukuoka 808-0135, Japan
Tel: +81-93-695-3294, Fax: +81-93-695-3368

June 27, 2020

Dear Dr. Laura Ghandhi,
Publishing Editor, Polymer Chemistry

Submission of the image of the potential back cover

We would like to submit the image associated with our article.

Manuscript title: Furry nanoparticles: Synthesis and characterization of nanoemulsion-mediated core crosslinked nanoparticles and their robust stability in vivo

The text for the image:

Nanoemulsion-mediated core crosslinked nanoparticles, named furry nanoparticles, are described in this cover. The nanoparticle can be easily and quickly prepared and shows robust stability in vivo.

We hope our image will be accepted as the back cover of ***Polymer Chemistry***.

Corresponding author's name and complete contact information: Dr. Shota Fujii
e-mail: s-fujii@kitakyu-u.ac.jp

Sincerely yours,

Dr. Shota Fujii

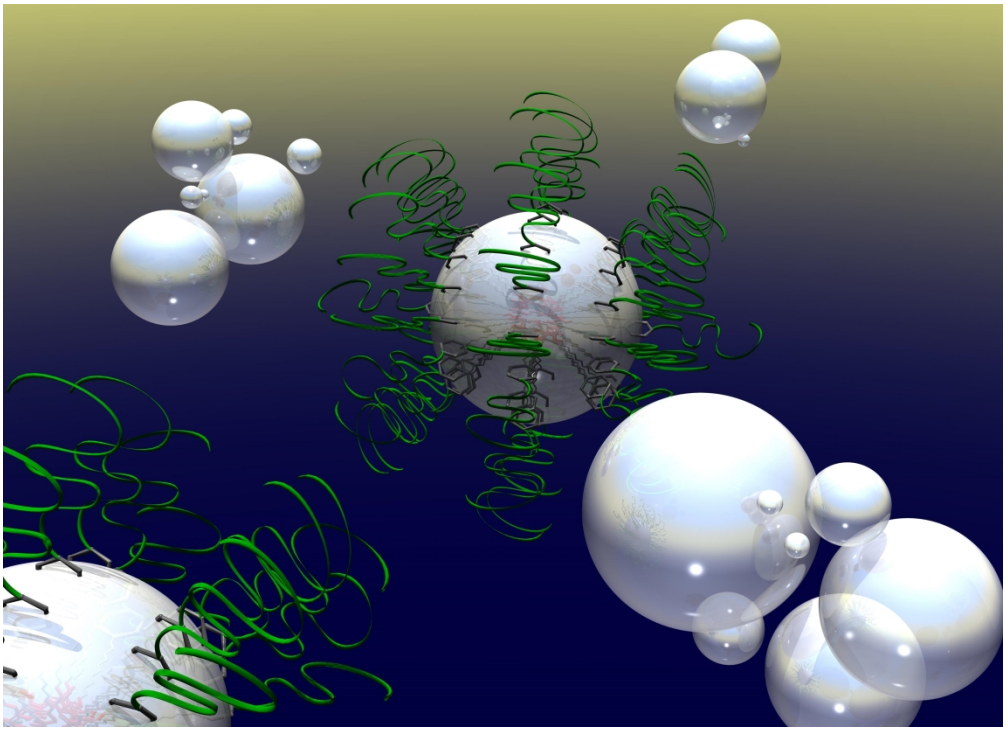

187x135mm (600 x 600 DPI)